Cr-doped Al 2 O 3 –YAG binary and Al 2 O 3 –YAG–ZrO 2 ternary eutectic materials crystallized by the micro pulling down technique and their characterization

J. Xu, Yannick Guyot, A. Nehari, A. Pillonnet, G. Ledoux, H. Takeda, X. Xiaodong, K. Lebbou

Cr-doped Al_2O_3-YAG binary and Al_2O_3-YAG-ZrO_2 ternary eutectic materials crystallized by the micro pulling down technique and their characterization

J. Xu[a], Y. Guyot[a], A. Nehari[a], A. Pillonnet[a], G.Ledoux[a], H. Takeda[b], X. Xiaodong[c], K. Lebbou[a]

[a]Institut Lumière Matière, UMR5306 CNRS, Université de Lyon 1, 69622 Villeurbanne, Cedex, France
[b] Graduate School of Science and Engineering, Saitama University, 255 Shimo-Okubo, Sakura-ku, Saitama 338-8570, Japan
[c] Jiangsu Key Laboratory of Advanced Laser Materials and Devices, School of Physics and Electronic Engineering, Jiangsu Normal University, Xuzhou 221116, China

Abstract

Cr-doped Al_2O_3-YAG and Al_2O_3-YAG-ZrO_2 eutectic ceramics rods of 3mm in diameter were solidified from the melt by micro-pulling down (μ-PD) technique. The Cr dopant affects the microstructure and the morphology and the lattice parameters of the as-grown eutectics. As a function of the dopant, the coloration, the morphology, microstructure, and the luminescence were investigated. Whatever the Cr-dopant concentration, mainly two phases (Al_2O_3-YAG) in case of binary system and three phases (Al_2O_3-YAG-ZrO_2) in case of ternary system were observed. The Chinese script microstructure, colony boundaries are observed in ternary eutectics. Al_2O_3 and YAG phases show faceted morphologies, but for ZrO_2 phase, growth tends to a weakly faceted manner and forms rods or lamellae. The hydrostatic stress of binary eutectics less than that of ternary eutectics with same Cr dopant concentration due to distribution of ZrO_2 particles in the microstructure affected the residual stresses. The spectroscopic properties of the Cr-doped binary and ternary eutectic show that Cr^{3+} ions exist in both Al_2O_3 and YAG phases in octahedral sites.

Key word: Eutectics; Cr, Color; Solidification; Microstructure; Luminescence

1. Introduction

Color eutectic ceramic materials have aroused a great attention in the innovation applications of Light-Emitting Diode (LED), watch pointer and jewelry decoration; it is required to produce higher quantity and performed more economic attributes [1-4]. The colored (red, blue, yellow…) ceramics have the ability to be used in jewelry and luxury and can substitute some specific crystal such ruby.

The eutectics ceramics materials offer technical characteristics in quality of hard material but also of scratch resistance, biocompatibility, insensitivity to any chemical attack, resistance to friction and abrasion, but also aesthetic advantages which intended for dressing applications [5-7]. The Al_2O_3-YAG binary and Al_2O_3-YAG-ZrO_2 ternary systems [8-11] are among the eutectics ceramics materials that are identified to be the most important composites materials due to directional and rapid solidification from the melt [12-13]. The high melting temperature > 1500°C, allowing them to work stably in oxidizing environment due to inherent chemical-physical properties [14]. They present excellent mechanical properties that are heavily dependent on the microstructure, morphology and crystallographic orientations [15-16] and are considered as potential engineering materials. It is well known that controlling uniform microstructure of the eutectic ceramics in the binary or ternary systems is related to the directionally solidification behavior that depended on the solidification methods and the specific composition in the equilibrium diagram [17-21].

Chromium oxides can be used in the ceramic because they are characterized by a large variety of colors. Therefore, chromium is an element of choice for obtaining colored minerals, since it colors many compounds in red, purple or green. It is in most cases in the form of Cr^{3+} in octahedral symmetry. Chromium is a transition element of electronic configuration for the metal Cr^0 [Ar] $4s^2$ $3d^4$, which gives it a wide variety of possible degrees of oxidation from 0 to +6 [22]. However, oxidation states +3 and +6 are the most commonly encountered in minerals and glasses. The Cr^{3+} gives rise to many colors, it is mainly found in octahedral geometry in minerals and is notably responsible for the green color of the emerald and the red color of ruby, but can also give purple as in stichtite [23, 24]. The presence of Cr^{3+} in more or less distorted octahedral geometry results in the presence of two main absorption bands in the visible range of its optical spectrum. The observed energy shifts of the absorption bands of the Cr^{3+} between the different minerals explain the different colorations, since the transmission window in the visible range is modified with these displacements. By the analysis of the ruby and the emerald, Vauquelin et al [25] discovers that chromium is responsible for the respective red and green colors of these two minerals.

The synthesis of colored eutectics ceramics compounds is not well controlled. For example, despite all efforts, it has never before been possible to produce eutectics ceramics bright red in color to be used for jewelry and watch pivot. The aim of this

paper is in particular to propose red colored Cr-doped Al_2O_3-YAG and Al_2O_3-YAG-ZrO_2 eutectic ceramic materials solidified by the micro-pulling down (µ-PD) technique allowing significantly expand the range of possible colors in the production of colored eutectic ceramics materials.

2. Experimental procedure

2.1 Crystal growth conditions

The starting materials were made from commercial high-purity (>99.99%), Cr_2O_3, Al_2O_3, Y_2O_3 and ZrO_2 powders. The powders were mixed in agate mortar at eutectic proportion according to the binary (80 mol%Al_2O_3/20mol%Y_2O_3) and the ternary (65mol%Al_2O_3 /16mol%Y_2O_3 /19mol%ZrO_2) eutectic composition. The detailed compositions of different prepared materials and references are shown in Table 1. The mixture was sintered at 1500℃ for 24 hours in air atmosphere. Eutectic ceramic rods were solidified from the melt using the micro-pulling down technique presented in previous work [11, 13, 15, 21]. Iridium crucible is used, it is tapped in its lower part with a capillary die of 3mm in diameter. The crucible is enclosed in a chamber swept with an oxygen-free argon stream, and is charged with eutectic ceramic raw materials. The crucible is brought to a temperature of 1750°C±2°C using a high frequency generator operating at 11 kHz and having a continuous power output of 25kw. When a pendant drops forms at the bottom of the capillary channel (Fig. 1), it is connected with a rod of eutectic ceramic of selected composition with diameter of 2mm to serve as the seed. When the drops weld to the seed, the seed is pulled down at a rate of 0.3mm.min^{-1}. A CCD camera was used to take inset a live picture through a small circular window (Fig. 1b). High-purity flowing argon was used to prevent oxidation of iridium crucible and after heater crucible support.

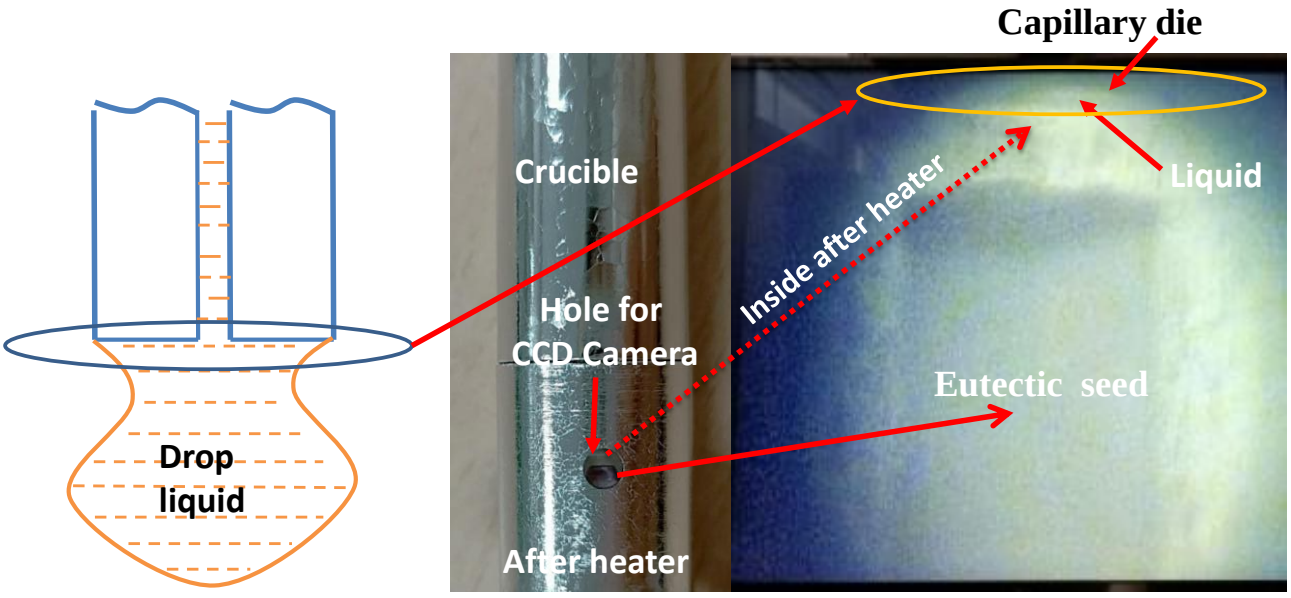

Fig. 1. Schematic illustration of the drop at the bottom of the capillary die (left), CCD camera vision of the growth initiation through the crucible and after heater (right)

Table 1. The different compositions used for melt solidification

	Binary Eutectic (Al_2O_3 (80%) / Y_2O_3 (20%))			
Sample (**Reference**)	Cr BE1	Cr BE2	Cr BE3	Cr BE4
Dopant	1.9at%	1.5at%	0.7at%	0.4at%
	Ternary Eutectic (Al_2O_3 (65%) / Y_2O_3 (16%) / ZrO_2 (19 %))			
Sample (**Reference**)	Cr TE1	Cr TE2	Cr TE3	Cr TE4
Dopant	1.9at%	1.5at%	0.7at%	0.4at%

2.2. Characterization methods

2.2.1. XRD phase analysis and Scanning electron microscopy

Room-temperature X-ray diffraction patterns were obtained using a Bruker D8 advanced diffractometer with Cu-Kα_1 and Cu-Kα_2 X-rays (λ=0.15406 and 0.15444 nm). The diffraction diagram is scanned over a 2θ range from 15°to 70° in steps of 0.02° with a counting time of 1 s per step and continuous rotation (20 rpm) for measurement. In order to investigate the formation and evolution of microstructures, the eutectic samples were cut and polished along the longitudinal and transversal, the pieces about 2 to 10 mm in length are embedded in organic resin. SEM observations of the polished samples were performed with a Phenom desktop scanning electron microscope (SEM) at 5 kV.

2.2.2. Spectroscopic characterizations

The fluorescence lines of ruby single crystals are used to evaluate the residual stresses in the solidified rods, the displacement of fluorescence line of chromium (Cr^{3+}) is measured. A 473 nm laser wavelength has been used as excitation source and focused on the surface of the polished samples through a 50X Olympus MIR plan objective with 0.25 NA in order to cover larger sample area. For each sample, a 121 point of measurement are taken on different areas of the polished transversal and longitudinal section, all the measured spectra are fitted using a Gaussian profile in order to determine the exact peak positions of Cr^{3+} fluorescence lines.

The emission spectra were registered at room (RT) and liquid nitrogen temperatures by exciting the crystals with an EKSPLA NT342B tunable OPO (Optical Parametric Oscillator) pumped by a pulsed and frequency-tripled Nd:YAG laser delivering 7 ns

laser pulses. Emission signals were dispersed and detected in the visible range with the aid of a SHAMROCK 350 monochromator equipped with both 300 line/mm and 1200 line/mm gratings, and an ANDOR ICCD gated detector. The high temperature measurements were performed using a LINKAM SCIENTIFIC cell DSC600 with an analogous Photo-Luminescence set-up.
The fluorescence decay measurements were performed by using the same laser excitation sources and a Jobin-Yvon HRS1 monochromator and by analyzing the signals with the help of R928 AsGa (RESEARCH Inc.) photomultiplier tubes coupled with a Wave Runner 64Xi LECROY digital scope, for the visible and NIR spectral ranges, respectively. The excitation spectra of Cr-doped Al_2O_3-YAG (binary system) and Al_2O_3-YAG-ZrO_2 (ternary system) eutectics in the range from 285 to 680 nm are recorded at room temperature with the help of an EDINBURGH Instruments FS5 spectrofluorimeter.

3. Result and discussion

3.1 Eutectic solidification and phase's characterization

As a function of the composition, the Cr doped binary (Al_2O_3-YAG) and ternary (Al_2O_3-YAG-ZrO_2) eutectic ceramics rods solidified from the melt are shown in Fig. 2. They were crystallized under stationary stable regime. Except the CrTE4 (0.4%Cr) sample, the Cr doped eutectic ceramics rods have a stable diameter of 3 mm. Whatever the system (binary or ternary), the red color contrast increase with increasing the Cr concentration. The variation in color coordinates (x,y) as presented in the CIE-1931 chromaticity diagram (Fig. 3) showing various red colors can be obtained by varying Cr concentration in the eutectic ceramics. The ceramics eutectics rods corresponding to high Cr concentration (1.9% Cr) have a strong red color close to the blood color. The surface of the samples is smooth without any visible macroscopic defects such as cracks or bubbles. Fig. 4a and 4b showed the XRD diagram of the eutectic ceramics as a function of Cr concentration for the binary and the ternary systems. The grinding of the material makes it possible to overcome the phenomena of texturing and distortion of cells due to the internal stresses of the material at room temperature. The YAG is identified as the majority phase in both systems. In the case of the Cr-doped Al_2O_3-YAG binary system, only Al_2O_3 and YAG phases are observed. Additional cubic ZrO_2 phase was crystalized in the case of the Cr-doped Al_2O_3-YAG-ZrO_2 ternary system. We did not registered the presence of $YAlO_3$ perovskite phase or inclusions belonging to the Al_2O_3, Y_2O_3, and Cr_2O_3 oxides indicating that Cr ions doping did not create impurities phases or induce a significant changes in the structure architecture. Table 2 present the lattice parameters as a function of the Cr concentration. In case of the YAG phase, whatever the system (binary or ternary), we registered a light increasing of the lattice parameter (a). The YAG has a garnet structure with Y^{3+} occupying a dodecahedral site and Al^{3+} ions occupying octahedral and tetrahedral sites, respectively [26]. The cells contains eight

groups form $Y_3Al_2Al_3O_{12}(X_3Y_2Z_3O_{12})$. The X, Y, and Z sites cations respectively occupy the positions 24c, 16a and 24d, and the anions are located at the positions 96h. The chromium (located on the Y sites) is therefore at oxidation state 3 and has a punctual symmetry 3^- or C3i in Schönflies notation. The Cr^{3+} substitutes $A1^{3+}$ in a small trigonally distorted octahedral site with Cj symmetry [27]. The structure of Al_2O_3 is the same as that of the Cr_2O_3. These two compounds form a complete solid solution, $Al_{2-x}Cr_xO_3$, by substitution of aluminum by chromium in octahedral site. The solid solution changes color with the chromium concentration. The introduction of a few tens of ppm of chromium replacing aluminum produces a characteristic pink color. The color intensifies with increasing chromium concentration, and as soon as the latter exceeds a few 0.7at% for both binary and ternary systems, the compounds acquire a strong red component. The color change of compounds is mainly due to changes in the parameter of crystal field Δ_0 [28,29]. Chromium dopant involving in the coloration being essentially in the form Cr^{3+} in more or less distorted octahedral symmetry. In addition, the broad absorption band peaking at 560 nm in the visible range is increasing with the Cr concentration, then for the highest Cr concentration the absorption at edge of this band for wavelength higher than 600 nm is also increasing giving to the sample a deep red color. Both binary and ternary eutectic ceramics rods contained Cr-doped α-Al_2O_3 phase belonging to the solid solution $Al_{2-x}Cr_xO_3$. Whatever the Cr concentration and the systems, all the solidified eutectic ceramic showed an increasing of a and c-lattices parameters in Cr-doped α-Al_2O_3 phase. This is principally due to the difference of the Cr^{3+} (61.5 pm) size which is considerably greater than the size of Al^{3+} (53.3 pm) [30]. The pics characteristics of $Al_{2-x}Cr_xO_3$ are therefore progressively shifted towards the lowest values of 2θ with Cr content (Fig. 4). In the case of the Cr-doped Al_2O_3-YAG-ZrO_2 system, we have not observed a variation of lattice parameter a in ZrO_2 phase. But the X-ray peaks of the cubic zirconia phase were shifted slightly because of some amount of Y_2O_3 was dissolved. On the basis of qualitative results under EDS, some amount of Y_2O_3 was contained in the ZrO_2 phase.

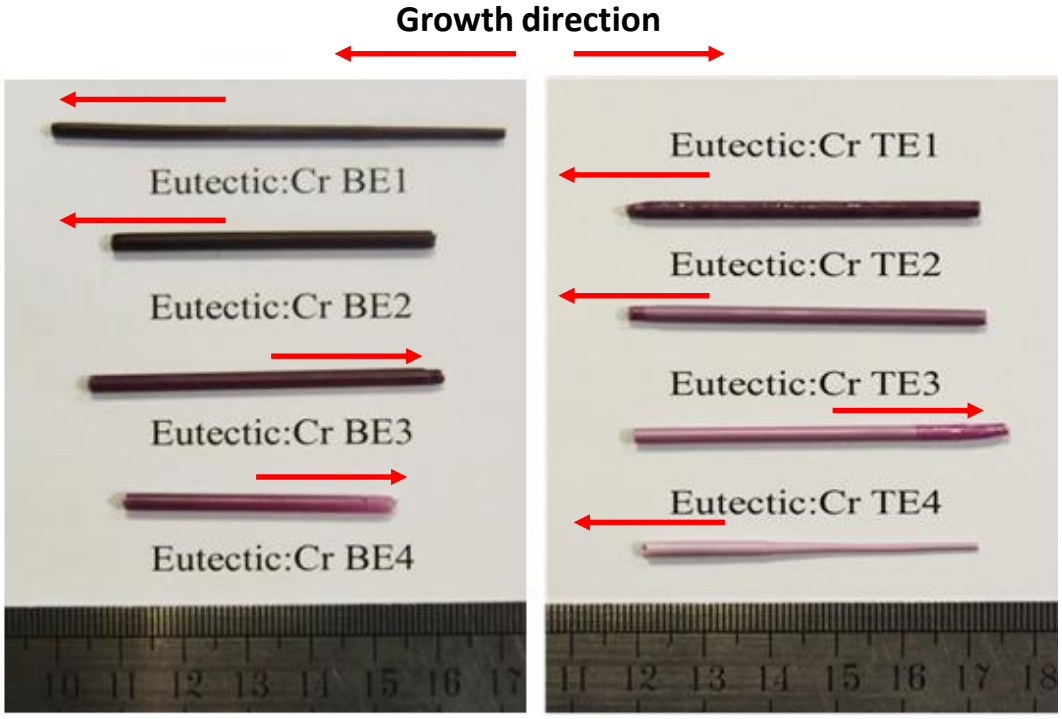

Fig. 2. Cr-doped eutectic ceramics solidified from the melt by μ-PD (pulling rate 0.3 mm/min)

CrBE1: Al_2O_3-YAG binary (Cr=1.9at%) CrBE2: Al_2O_3-YAG binary (Cr=1.5at%)

CrBE3: Al_2O_3-YAG binary (Cr= 0.7at%) CrBE4: Al_2O_3-YAG binary (Cr=0.4at%)

CrTE1: Al_2O_3-YAG-ZrO_2 Ternary (Cr=1.9at%) CrTE2: Al_2O_3-YAG- ZrO_2 Ternary (Cr=1.5at%)

CrTE3: Al_2O_3- YAG-ZrO_2 Ternary (Cr= 0.7at%) CrTE4: Al_2O_3-YAG ZrO_2 Ternary (Cr=0.4at%)

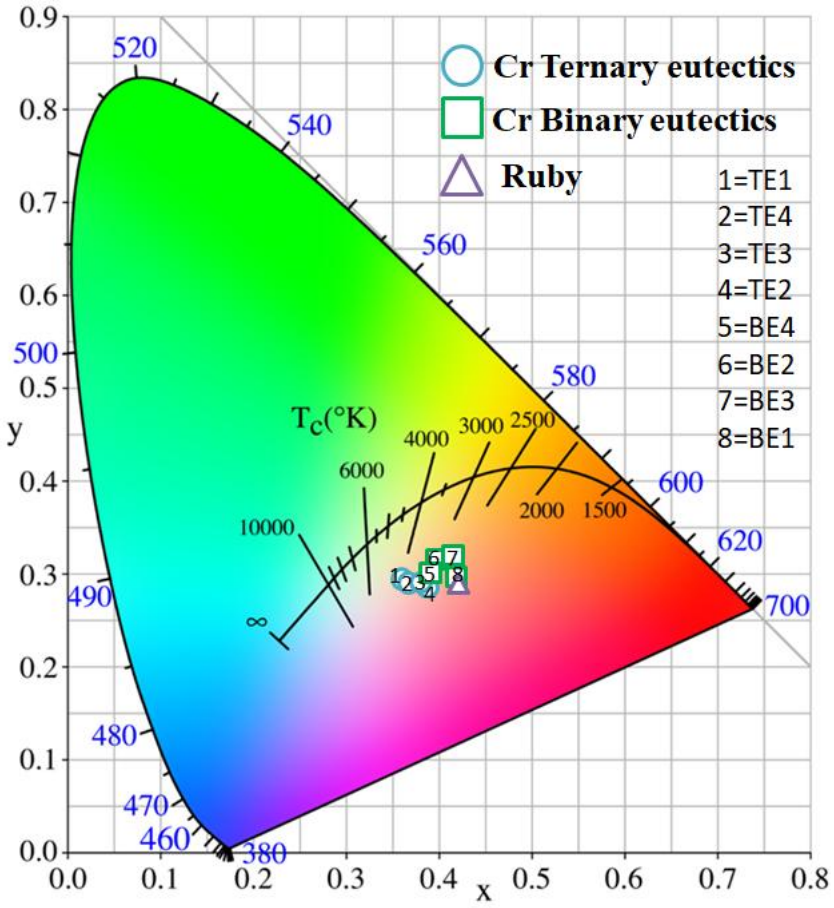

Fig. 3. CIE-1931 chromaticity diagram as a function of Cr concentration in the binary and the ternary eutectic

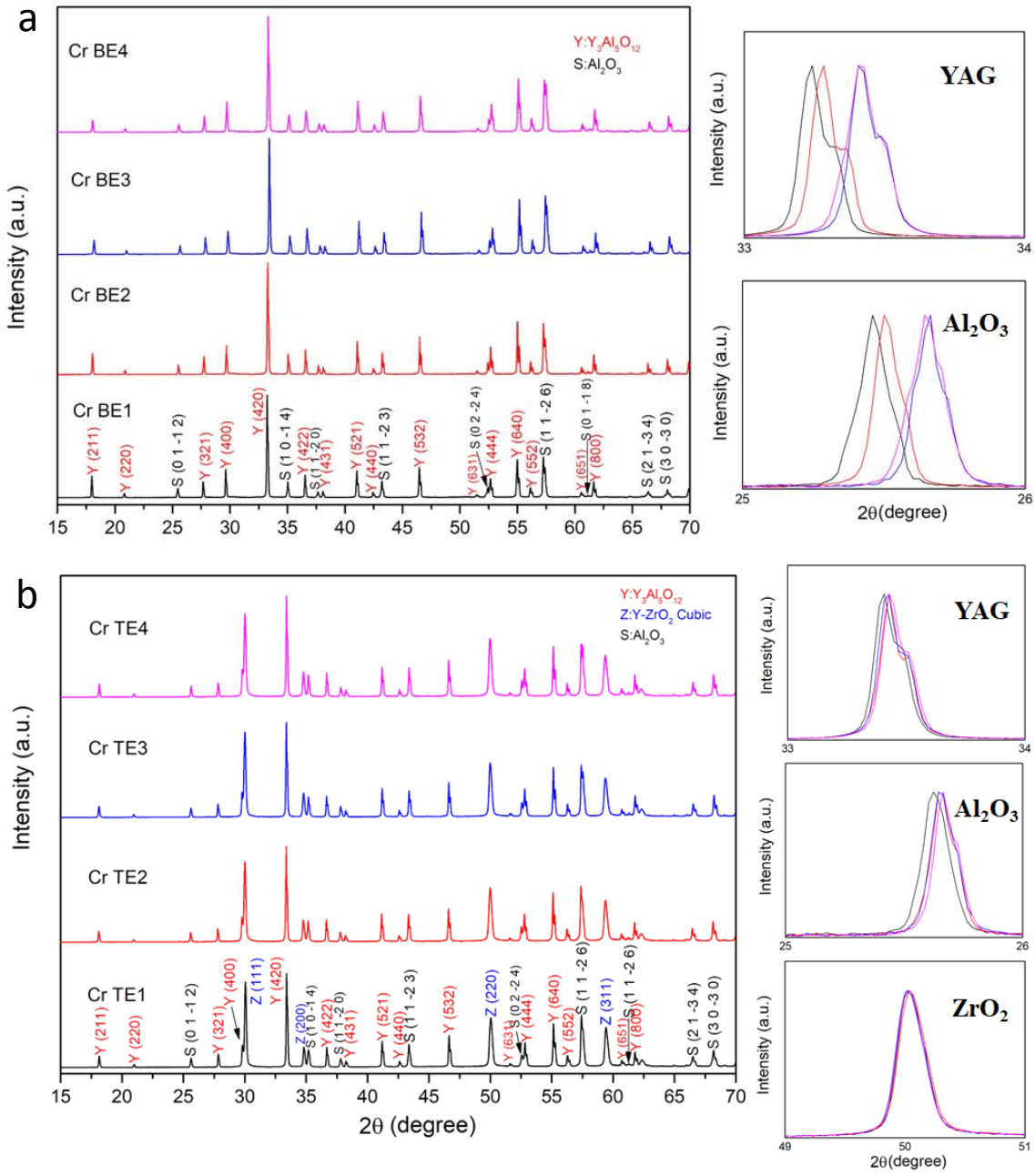

Fig. 4. X-ray diffraction evolution as a function of Cr dopant concentration, (a) Al_2O_3-YAG binary system and (b) Al_2O_3-YAG-ZrO_2 ternary system.

Table 2. Lattice parameters of Cr doped Al_2O_3-YAG/Al_2O_3-YAG-ZrO_2 as a function of the dopant concentration

	Al_2O_3 R-3c (Å)	$Y_3Al_5O_{12}$ Ia-3d (Å)	ZrO_2 Fm-3m(Å)
PDF files	a= 4.7585,c= 12.9906	a=12.0020	
Cr BE1	a=4.7648, c=13.0074	a=12.0139	
Cr BE2	a=4.7624, c=12.9999	a=12.0110	
Cr BE3	a=4.7624, c=13.0017	a=12.0130	
Cr BE4	a=4.7608, c=12.9935	a=12.0094	
Cr TE1	a=4.7650, c=13.0072	a=12.0123	a=5.1605
Cr TE2	a=4.7642, c=13.0037	a=12.0135	a=5.1619
Cr TE3	a=4.7611, c=12.9957	a=12.0093	a=5.1625
Cr TE4	a=4.7602, c=12.9955	a=12.0084	a=5.1628

Fig. 5 and Fig. 6 show the SEM images of the transverse and the longitudinal sections cut from the Cr-doped Al_2O_3-YAG binary and Al_2O_3-YAG-ZrO_2 ternary eutectic ceramic rods. The precise knowledge of the solidification conditions, namely solidification rate and initial composition, makes it possible to study the influence of these different parameters on the morphology. The addition of the Cr in the binary Al_2O_3-YAG system do not strongly affect the architecture morphology of this system. Unlike the ternary system, the binary eutectic present a homogeneous microstructure for all the Cr concentration.

It is composed of two phases distinguished by their different sharps and colors, the black regions correspond to the α-Al_2O_3 phase and the grey regions correspond to YAG ($Y_3Al_5O_{12}$) phase. The Al_2O_3 is the matrix and the YAG phases are disconnected on transverse sections to the solidification direction. The shape and size of the YAG phase are irregular. The longitudinal sections (Fig. 6) show that the microstructure is irregular lamellar and correspond to Chinese Script microstructure. The lamellae are elongated along the solidification direction. The YAG size increase with Cr concentration increasing and reach a maximum average around 40 µm for 1.9at% Cr (Fig. 6d). The coarsening as a function of Cr concentration is quite homogeneous and the microstructure remained unchanged. In the binary system, the dimension, the homogeneity and the morphology of the microstructure are modified by varying the Cr concentration. A high Cr concentration promotes the contribution of the diffusion leading to an increase in the size of the microstructure. Increasing Cr concentration is similar to decreasing pulling rate in Al_2O_3-YAG system [26]. The microstructure corresponding to the lower Cr concentration (0.4at %) is much finer. In eutectic solidified with low Cr concentration smaller phase sizes, the diffusion was enhanced.

It is registered a significant coarsening of the fine microstructure. It seems that the coarsening process is Cr^{3+} diffusion through $Y_3Al_5O_{12}$ and Al_2O_3.

The Cr- doped Al_2O_3-YAG-ZrO_2 system the microstructure is composed of three phases, Al_2O_3, YAG and ZrO_2. The main phases are YAG and alumina, which respectively have volume fractions of 42 vol% and 40 vol% (Fig. 6). The zirconia phase is distributed mainly at the interface of the alumina and YAG phases or in the alumina phase with 1-5µm. Intragranular ZrO_2 with very small (0.1-0.8 µm) size rounded YAG phase. The longitudinal sections of the solidified samples show a "broken" or irregular lamellar microstructure. The lamellae are elongated along the solidification direction. In the ternary system, as a function of Cr concentration from 0.4 to 1.9 at%, we did not registered an increasing of YAG grains and magnification of the microstructure as observed in the Al_2O_3-YAG binary system. The microstructure of the ternary system is finer and with more curved interfaces than that of the Cr-doped Al_2O_3–YAG eutectic system solidified at the same rate. Whatever the Cr concentration (0.4-1.9at %), the homogeneous character disappears giving way to a colonies apparition but the microstructures are interconnected. Both YAG and ZrO_2 phases in the Cr-doped ternary eutectics showed different morphology than in their respective Al_2O_3-based binary eutectic system [31,32,33], but Cr addition don't affect the shape of ZrO_2 particle and the script size of the YAG phase was found to be uniform for each cross section investigated. The SEM observations show that the Cr doping in the ternary system leads, in our case, to an excess of YAG (in grey) marked by the formation of large primary crystals. The Al_2O_3 phase (black) is also slightly in excess compared to the garnet phase (grey).

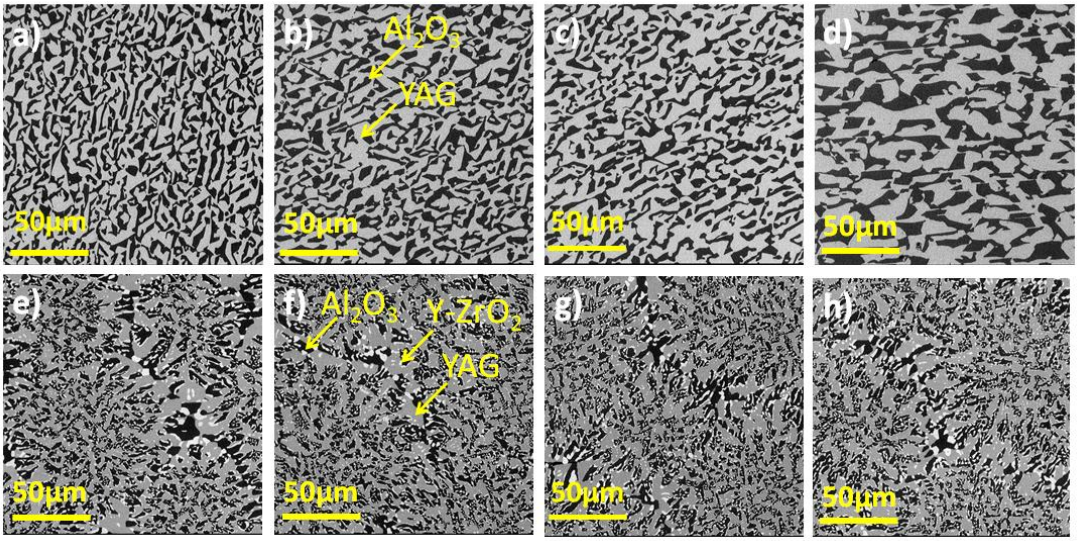

Fig. 5. Transversal microstructure evolution as a function of concentration. (a) binary eutectic Cr 0.4at%, (b) binary eutectic Cr 0.7at%, (c) binary eutectic Cr 1.5at%, (d) binary eutectic Cr 1.9at%, (e) ternary eutectic Cr 0.4at%, (f) ternary eutectic Cr 0.7at%, (g) ternary eutectic Cr 1.5at%, (h) ternary eutectic Cr 1.9at%.

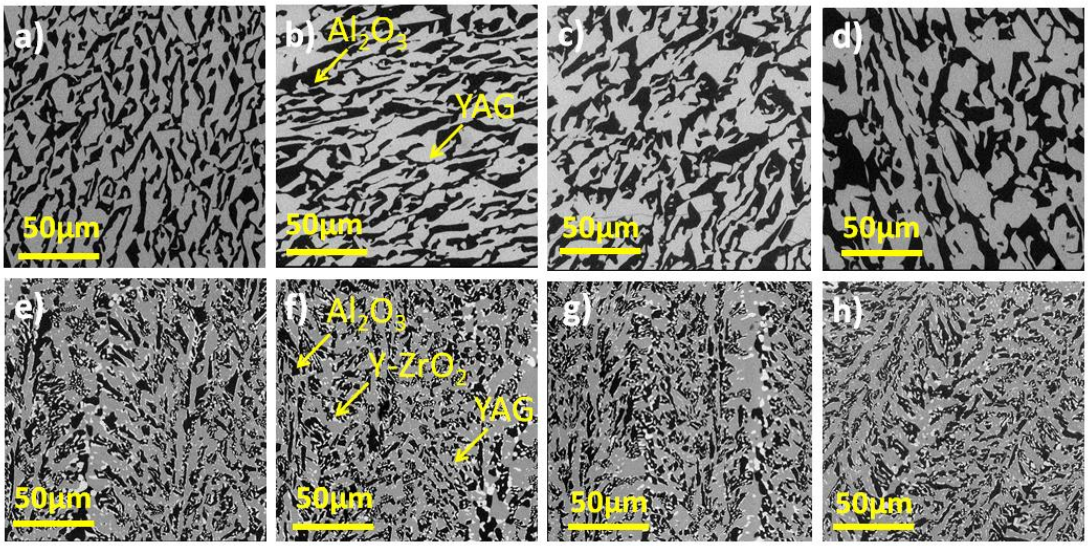

Fig. 6. Longitudinal microstructure evolution as a function of concentration. (a) binary eutectic Cr 0.4at%, (b) binary eutectic Cr 0.7at%, (c) binary eutectic Cr 1.5at%, (d) binary eutectic Cr 1.9at%, (e) ternary eutectic Cr 0.4at%, (f) ternary eutectic Cr 0.7at%, (g) ternary eutectic Cr 1.5at%, (h) ternary eutectic Cr 1.9at%.

3.2 Residual stress

The thermal elastic residual stresses of eutectics in the solidification process is caused by different thermal expansion mismatch between the α-Al_2O_3, YAG and ZrO_2:Y phase [26,34].The fluorescence of Ruby single crystal is taken as reference to measure the residual stresses due to the electronic Cr^{3+} levels is characterized by R1 an R2 luminescence lines, in most instances, the R2-line shift could be used to calculate approximate values of the hydrostatic stress σ_h, the relation follows [35,36]:

$$\Delta\nu_2=7.61\sigma_h,$$

Where $\Delta\nu_2$ refers to the peak shift of R2-line (expressed in units of cm^{-1}) and σ_h present the hydrostatic stress given in units of GPa. Fig. 7 and Fig. 8 shows the fluoresce spectra of Cr^{3+} present in the in the alumina phase of Cr doped Al_2O_3-YAG/Al_2O_3-YAG-ZrO_2 solidified eutectic. The evolution of the average hydrostatic stress measured on the transversal and longitudinal section of the samples is shown in Fig. 7 and Fig 8, the negative values of the hydrostatic stress indicate that the alumina phase is under compression, which is observed in references [7,37]. Whatever the transversal and longitudinal microstructure, the hydrostatic stress of binary eutectics less than that of ternary eutectics with same doped concentration due to distribution of ZrO_2 particles in the microstructure affected the residual stresses. The higher concentration of Cr-doped eutectic of Chinese script morphology is less compressed than that of lower concentration. In a word, the variation of the residual stresses of Cr doped Al_2O_3-YAG/Al_2O_3-YAG-ZrO_2 solidified eutectics, which not only depends on the cooling rate and time but also affected by the dopant and the concentration (Fig. 9).

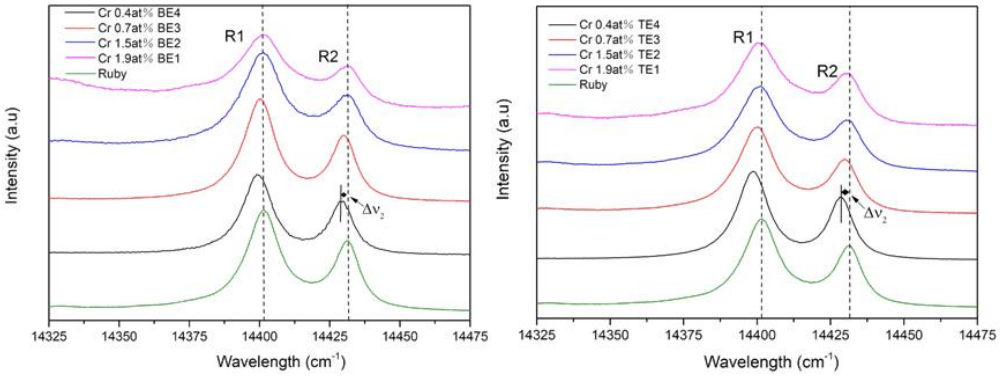

Fig. 7.Ruby fluorescence (R1 and R2 bands) excited with a 473 nm laser in transversal sections of the eutectics as a function of concentration.

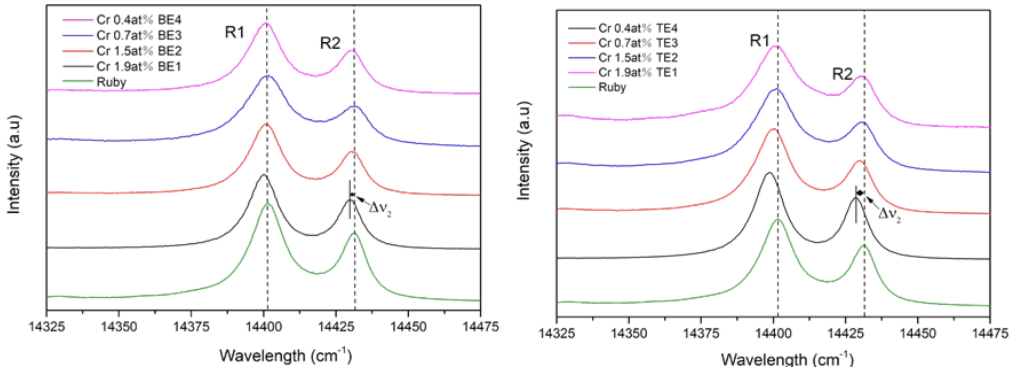

Fig. 8. Ruby fluorescence (R1 and R2 bands) excited with a 473 nm laser in longitudinal sections of the eutectics as a function of concentration.

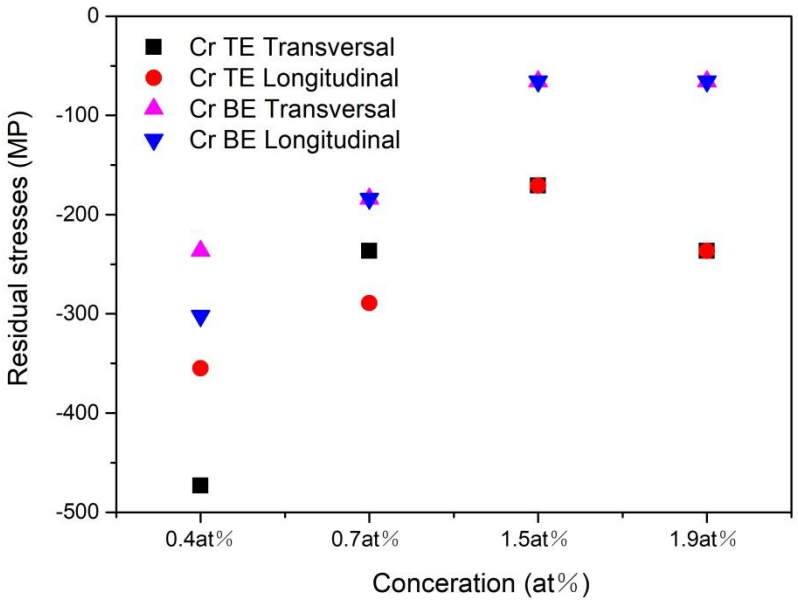

Fig. 9. Variation of the residual stresses (transversal and longitudinal sections) as a function of concentration according to Cr doped binary and ternary eutectics

3.3 Emission and excitation spectra

The room temperature (300K) emission spectra of Cr-doped Al_2O_3-YAG/Al_2O_3-YAG-ZrO_2 eutectics in the wavelength range of 600-900 nm are recorded under green (532 nm) and blue excitation light (450 nm) are shown in Fig. 10. Under the green excitation, Cr-doped Al_2O_3 is clearly identified [38]. The sharp line centered at 694 nm corresponds to the forbidden transitions spin from ^2E to $^4A_2$ level, referred to R-line, and the broad band centered at 774 nm is due to the phonon-assisted $^4T_2$ to ground state $^4A_2$. This last transition was mostly observed when Cr-doped Al_2O_3 is higher than 0.5 at%. Indeed, the relative intensity of broad band centered at 774 nm is increasing with the concentrations [38]. This effect is magnified in Cr-doped ternary eutectics. Moreover, under the blue excitation, an additional sharp line around 688 nm appears; it is attributed to the $^2E \rightarrow {}^4A_2$ transition of Cr-doped YAG phase [39].

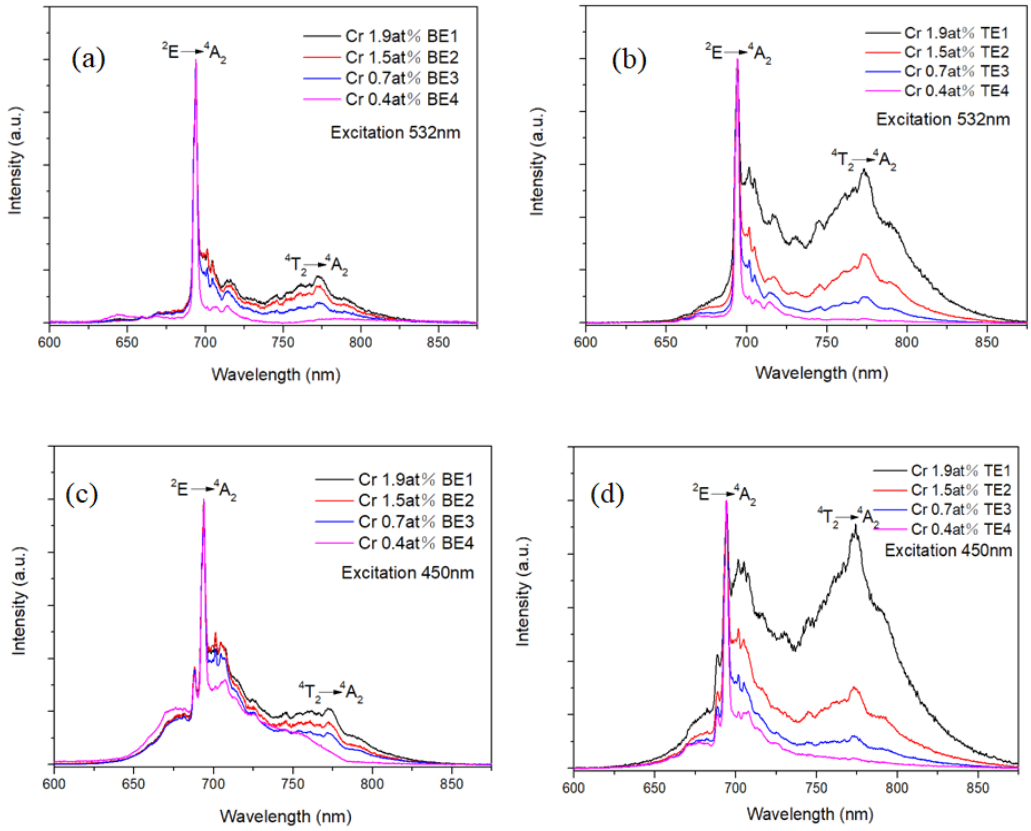

Fig. 10. The room temperature (300K) emission spectra of eutectics (a) Cr-doped binary eutectics under excitation at 532 nm. (b) Cr-doped ternary eutectics under excitation at 532 nm. (c) Cr-doped binary eutectics under excitation at 450 nm. (d) Cr-doped ternary eutectics under excitation at 450 nm.

The low temperature (77K) emission spectra of Cr-doped binary and ternary eutectics in the wavelength range of 680-850 nm were recorded also under excitation at 532 and 450 nm excitation as shown in Fig. 11. The broad emission band with peaks at 774 nm is observed due to $^4T_2 \rightarrow {}^4A_2$ transition, in good agreement with R.C. Powell et al. [40]. At low temperature, the $^4T_2$ emission band is more structured but remains as

large as at RT, however, the effect of decreasing temperature strongly affects the structure of the spectra in the 690-710 nm range: splitting of the Cr:Al_2O_3 R lines and magnification of the doublet observed in its edge around 700 nm.

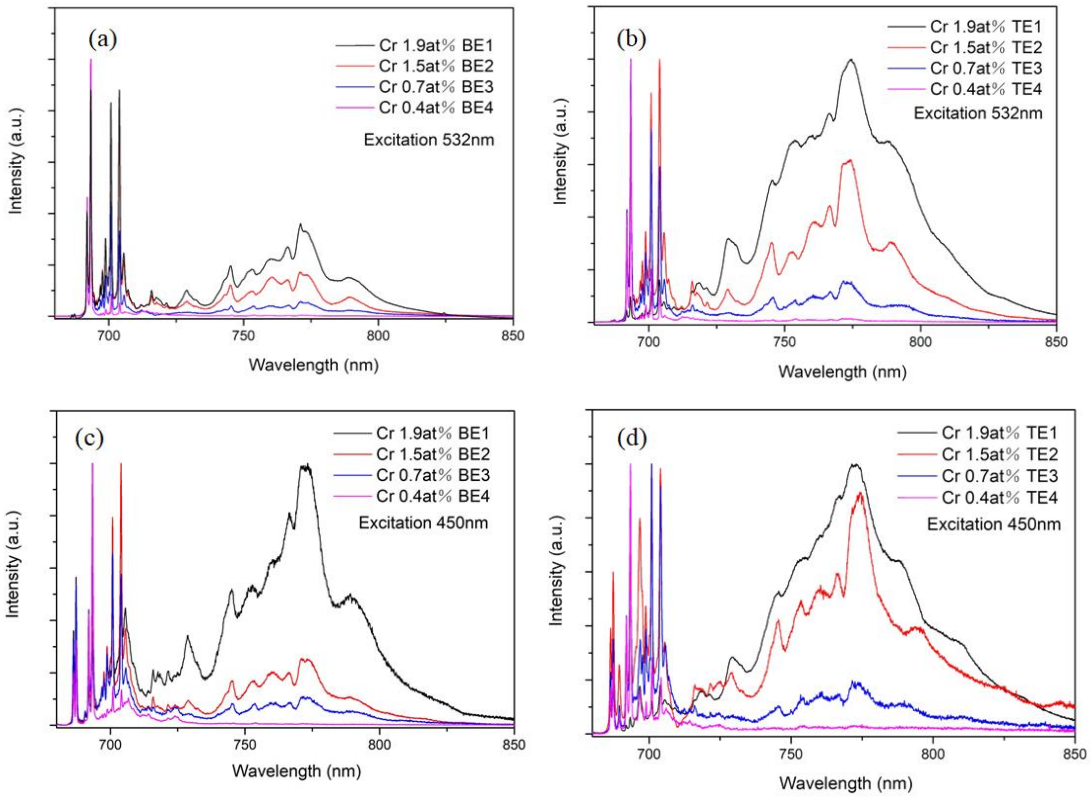

Fig. 11. The low temperature (77 K) emission spectrum of eutectics (a) Cr-doped binary eutectics under excitation at 532 nm. (b) Cr-doped ternary eutectics under excitation at 532 nm. (c) Cr-doped binary eutectics under excitation at 450 nm. (d) Cr-doped ternary eutectics under excitation at 450 nm.

In order to analysis the rich luminescence spectrum in this range, the emission covering the spectral range from 680 nm to 710 nm is shown Fig.12. Under green excitation at 532 nm, the first sharp lines lying at 693.4 nm and 692.0 nm are assigned to R1 $\bar{E}\rightarrow{}^4A_2$ and R2 $\bar{A}\rightarrow{}^4A_2$ lines, respectively, due to the spin-orbit coupling and then, the splitting of the radiative transition $^2E\rightarrow{}^4A_2$ in Cr^{3+} ions in octahedral crystal field [41-42]. Whereas, the second doublet of sharp lines at 704.0 nm and 700.9 nm corresponds to Cr^{3+}-Cr^{3+} pair lines which are designated N1 and N2 in Al_2O_3, respectively [40]. The ratio between the N and R-line intensity slightly increases in the ternary eutectics.

In addition, under blue excitation (450 nm), a third doublet of sharp lines appears at 686.3 nm and 687.3 nm corresponding to the splitting of Cr R line in YAG. The relative intensity of N lines and R lines increases with the Cr concentration as expected. Under 532 nm excitation, no difference between ternary and binary eutectics emission spectra is observed whereas under 450 nm excitation at least two additional lines appear 689.5 nm and 696.7 nm in the ternary compound coming from

Cr-doped YAG phase. Indeed under selective excitation in the 685-700 nm range, these additional lines only appear when excited in the two 687.3 and 686.0 nm Cr-YAG R lines.

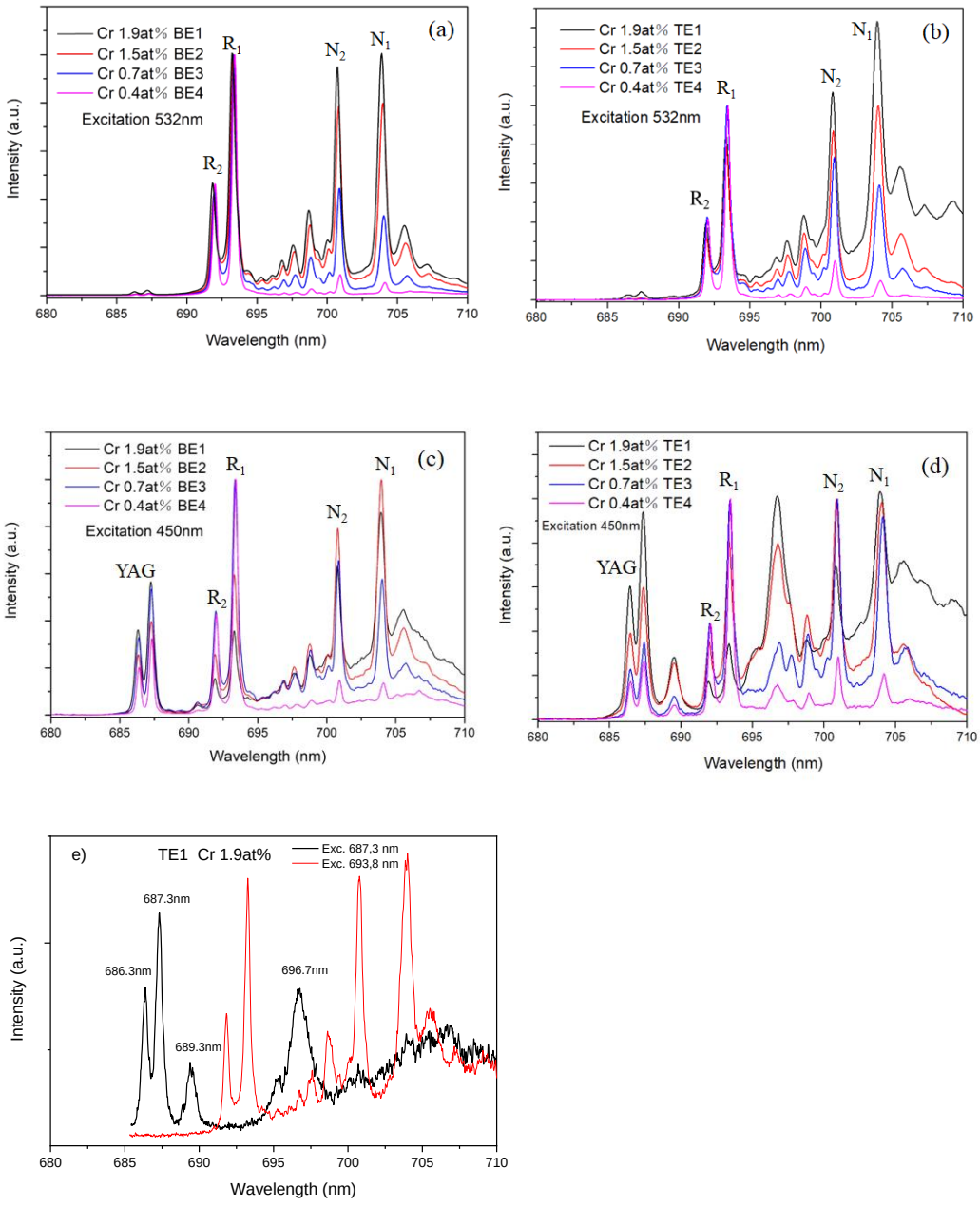

Fig. 12. The low temperature (77 K) emission spectrum of eutectics range from 680 nm to 710 nm under excitation at 532 nm a), b); 450 nm c), d) and selective excitations at 694.2 and 687.3 nm e).

The high temperature emission spectra of eutectics from 315 to 673 K are shown in Fig. 13. Under 532 nm excitation of the Cr in the alumina phase, when the temperature is increasing, the $^4T_2$ level becomes more and more thermally populated then the intensity of the broadband is increasing relatively to the line (694 nm)

corresponding to the $^2E \rightarrow {}^4A_2$ emission. Under excitation of 450 nm, the line at 688 nm, $^2E \rightarrow {}^4A_2$ of Cr in YAG-phase, rapidly disappears (at already 100°C). Indeed when the temperature increases, the both $^4A_2 \rightarrow {}^4T_2$ and $^4A_2 \rightarrow {}^4T_1$ absorption or excitation bands, shown in the Fig. 14, become much broader and then, at 450 nm the excitation of Cr in alumina phase is enhanced. This result points out that the high temperature measurements corroborate that the majority of Cr^{3+} ion entered favorably in the Al_2O_3 phase than in the YAG phase. This behavior is observed in both ternary and binary eutectics.

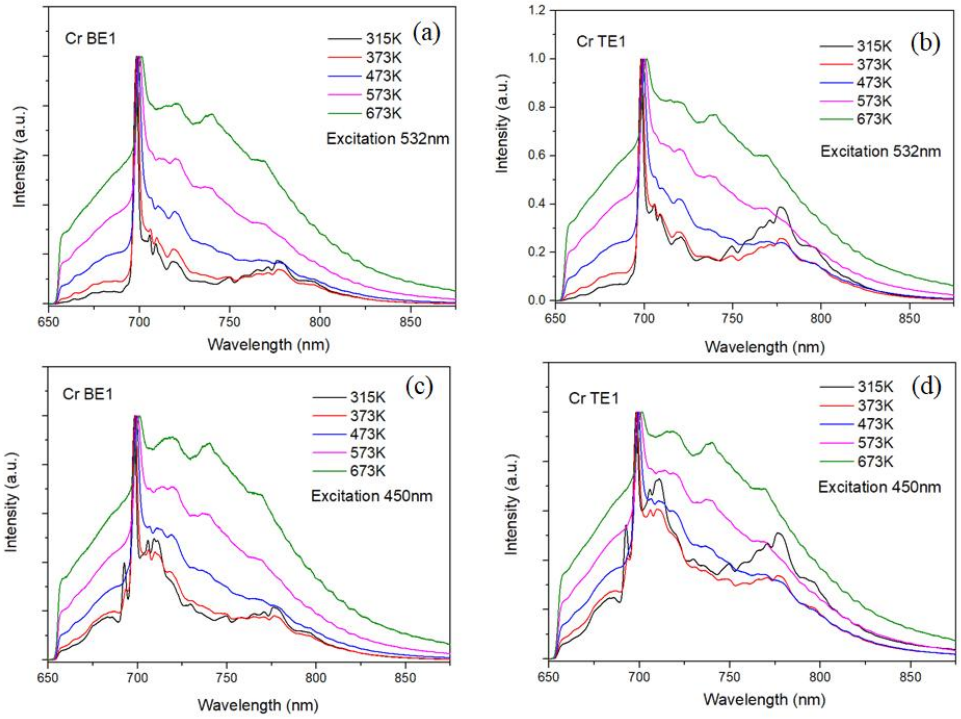

Fig. 13. High temperature emission spectrum, using a long-pass filter at 650 nm, of eutectics from 373 to 673 K (a) Cr-doped binary eutectic under excitation at 532 nm. (b) Cr-doped ternary eutectic under excitation at 532 nm. (c) Cr-doped binary eutectic under excitation at 450 nm. (d) Cr-doped ternary eutectic under excitation at 450 nm.

The room temperature excitation spectra of Cr-doped Al_2O_3-YAG (binary system) and Al_2O_3-YAG-ZrO_2 (ternary system) eutectics in the range from 285 to 680 nm are shown in Fig. 14. The excitation spectrum consists of two broad bands assigned to the $^4A_2 \rightarrow {}^4T_1$ (Y-band) as well as $^4A_2 \rightarrow {}^4T_2$ (U-band) spin-allowed transitions [43]. By monitoring the emission at 694 nm of Cr in Al_2O_3 phase the excitation bands are centered around 400 nm and 560 nm, while by monitoring the emission at 688 nm of Cr in YAG phase, these bands are both red-shifted and centered around 450 nm and 610 nm respectively. In addition, sharp excitation bands centered around 660 nm are corresponding to transitions from the $^4A_2$ ground state to $^2T_1$ level above ^2E. In the fig 14c, the asymmetrical shape of the excitation band is due to the overlap of the high energy part of the $^4T_2 \rightarrow {}^4A_2$ emission transition of Cr in the Al_2O_3 phase, then it is not

possible to select only the Cr luminescence in the YAG phase, this observation being more noticeable in Fig. 11d in the case of the ternary eutectics.

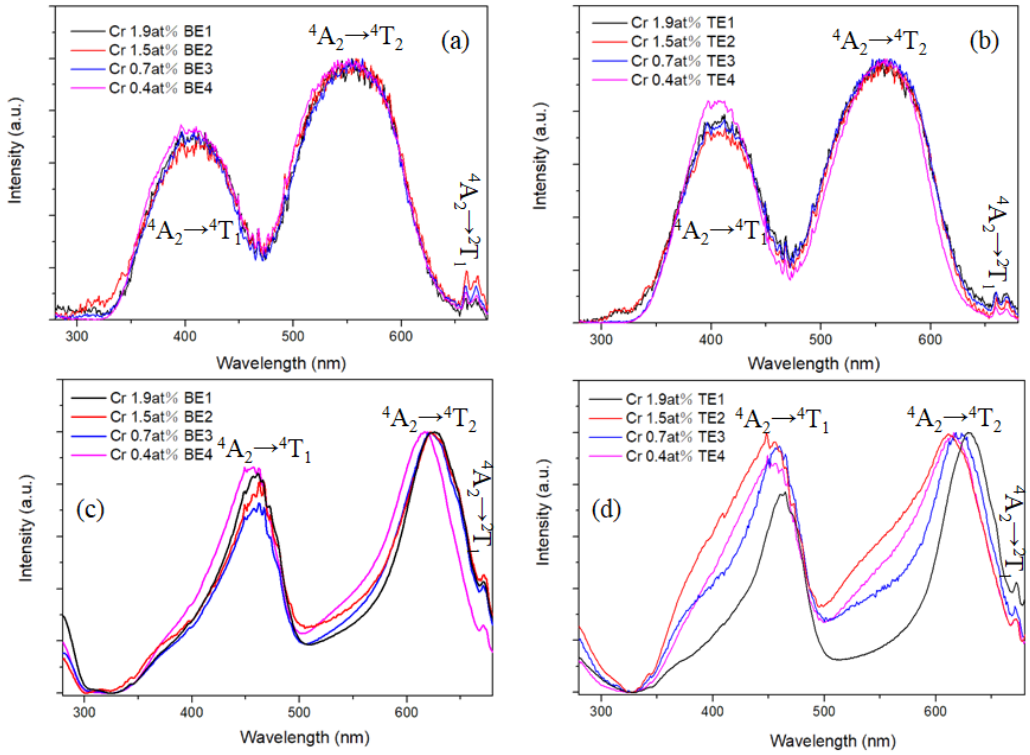

Fig. 14. Excitation spectrum of eutectics at room temperature (a) Cr-doped binary eutectics by monitoring the emission at 694 nm. (b) Cr-doped ternary eutectics by monitoring the emission at 694 nm. (c) Cr-doped binary eutectics by monitoring the emission at 688 nm. (d) Cr-doped ternary eutectics by monitoring the emission at 688 nm.

3.4 Fluorescence decay times

The fluorescence decay curves of the chromium luminescence as a function of the Cr concentration were recorded under 532 and 450 nm excitation at 300K and 77K, then the lifetime constants are gathered in Table 3 and Table 4 respectively. As the decay curves become non-exponential for the two highest concentrations as shown in the fig. 15 we calculated the integrated lifetime. As expected, at RT, the long lifetimes of the Cr^{3+} R-line $^2E \rightarrow {}^4A^2$ spin forbidden transition at 694.3 nm in Al_2O_3 phase is decreasing from 3.84 ms to 0.94 ms when the concentration increases from 0.4 to 1.9 at. % Cr-doped for the binary eutectics. The concentration quenching effect in more pronounced in Cr-doped ternary, the lifetime being as short as 0.21 ms for 1.9 Cr at. %. This behavior is also noticeable when comparing luminescence decays of the broad band centered at 774.3 nm in the binary and ternary systems. For this wavelength, the decay curves are particularly non-exponential due to the competition of the relaxation process from the excited level to the emitting $^4T_2$ level and the partial thermal equilibrium with the ^2E levels. However, this thermal coupling being less

efficient at low temperature (77 K), it is observed that the values of decay times of the $^4T_2 \rightarrow {}^4A_2$ allowed transition measured at 773.0 nm becomes shorter than at 300 K. Finally, the decay time of Cr-doped binary eutectics is in good agreement with Cr^{3+}:Al_2O_3 powder [38], and Ruby bulk crystals [40] especially considering the lifetime of about 1ms for 2 at% of the Cr-Cr pair emission of the N-lines measured at 704nm under 532 nm at low temperature. It is interesting to note that the lifetime of the emission of Cr pairs is much shorter in the ternary 0.3ms than in the binary eutectics 0.8 ms.

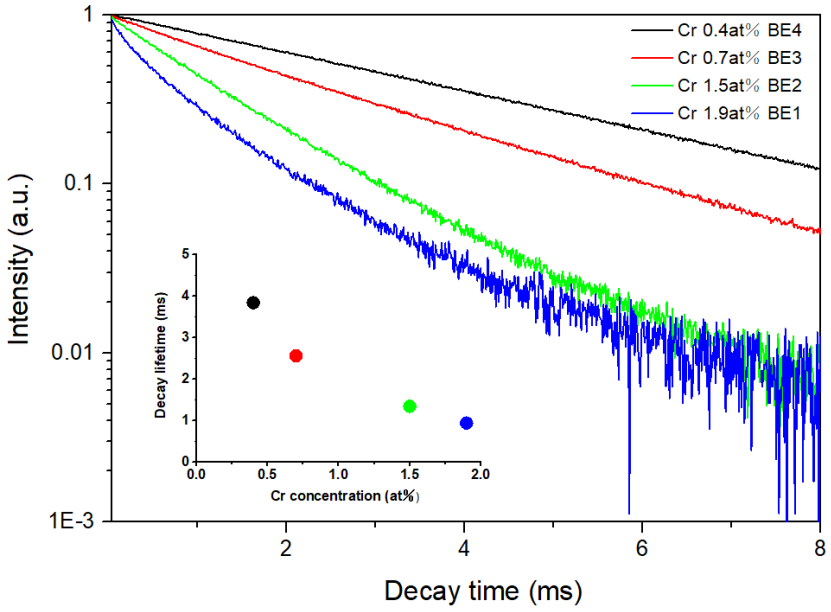

Fig.15 Fluorescence decay curves of the 694.3 nm emission under 532 nm excitation in Cr-doped binary eutectics at RT.

Now considering the luminescence decay time of Cr-doped YAG phase at 687.3 nm recorded under 450 nm excitation , the lifetime at 77 K binary eutectic is measured about 7.28 ms for 0.4 at. % Cr-doped, then it is a little smaller than the 8.8 ms measured in 0.05% at 7 K [39,44] but is slightly longer than that measured here in the Al_2O_3 phase in the same sample. It can be explained by a lower intermediate ligand crystal field strength Dq/Bp <2.1 in YAG [45] than in Al_2O_3 (Dq/B>2.33) [46] while the Cr^{3+} octahedral sites are slightly distorted [27] in YAG. At room temperature the lifetime 1.77 ms in both binary and ternary eutectics is in total agreement with the value given by Bray et al [39,45]. From table 2 and 3, one can note that the temperature quenching effect is stronger for the YAG phase than in ruby-phase while the phonon energy cutoff is rather the same , 865 cm^{-1} and 910 cm^{-1} [47] respectively. In the contrary the concentration quenching is larger in Al_2O_3 than in the YAG phase, indeed the lifetime decreasing ten times between the highest and the lowest concentration at 77 K in Al_2O_3, and only three times in YAG. It suggests that the concentration of Cr in the YAG-phase should be lower than in Al_2O_3-phase due to a lower segregation coefficient in YAG .Finally, as for Cr in Al_2O_3 phase, the decays become also shorter in the ternary compound for Cr in the YAG phase possibly

because of the higher Cr concentration in ternary eutectics as already suggested from the analysis of the emission spectra or by the decay curves of the N-line emission of pairs. Finally, the dynamics of the new emission lines at 689 and 696 nm is the same as the Cr luminescence in the YAG-phase.

Table 3. The decay times (in ms) of various emission under excitation 450 nm and 532 nm at 77 K.

	Excitation 532 nm		Excitation 450 nm
Sample	694.3 nm	774.3 nm	688.7 nm
Cr BE1	0.94	0.55	1.30
Cr BE2	1.34	1.24	0.95
Cr BE3	2.56	1.60	1.63
Cr BE4	3.84	-	1.78
Cr TE1	0.21	0.09	0.33
Cr TE2	0.63	0.97	0.64
Cr TE3	1.29	0.92	1.33
Cr TE4	3.30	1.08	1.77

Table 4. The decay times (in ms) of various emission under excitation 450 nm and 532 nm at 77 K.

	Excitation 532 nm			Excitation 450 nm
Sample	694.3 nm	704.0 nm	773.0 nm	687.3 nm
Cr BE1	0.74	0.81	0.61	4.80
Cr BE2	0.56	0.81	0.72	3.10
Cr BE3	2.10	1.87	1.08	6.27
Cr BE4	6.13	4.37	0.97	7.28
Cr TE1	0.30	0.26	0.30	1.67
Cr TE2	0.19	0.28	0.54	2.04
Cr TE3	0.77	0.80	0.62	5.54
Cr TE4	3.92	3.81	1.34	6.21

4. Conclusion

In this work, Cr-doped Al_2O_3-YAG binary and Al_2O_3-YAG-ZrO_2 ternary systems of eutectic ceramics were solidified from the melt by using the μ-PD technique. The coloration, the morphology and microstructure, the residual stress and the luminescence have been investigated. As a function of Cr-dopant concentration and

the binary or ternary system, the relationship between the microstructure and the optical properties and, as a result, solidified eutectic ceramic with optimized microstructures have been elaborated The Cr-doped eutectics present a red color. Whatever the dopant concentration, mainly two phases (Al_2O_3-YAG) in case of binary system and three phases (Al_2O_3-YAG-ZrO_2) in case of ternary system are observed. The Chinese script microstructure, colonies and colony boundaries are observed in ternary eutectics. From the different size of YAG grains, the microstructure formation of binary eutectics depends on the chromium dopant concentration. Moreover, Al_2O_3 and YAG phases show faceted morphologies, but for ZrO_2 phase, growth tends to a weakly faceted manner and forms rods or lamellae. Whatever the Cr dopant concentration, the hydrostatic stress of the binary eutectics are less than that of ternary eutectics.

The spectroscopic properties of the Cr-doped eutectic clearly show that Cr^{3+} ions enter in both Al_2O_3 and YAG phases in octahedral site. The increase of the intensity of the $^4T_2 \rightarrow {}^4A_2$ emission band relatively to the $^2E \rightarrow {}^4A_2$ lines, in one hand, and the intensity ratio between the N-lines and R-lines recorded at 77K, in the other hand, shows that the Cr concentration in Al_2O_3 phase should be higher in the ternary eutectic that in the binary eutectic. The analysis of the emission lifetime in both compound corroborate this observation: the luminescence quenching by concentration is emphasis in the ternary eutectics. Furthermore, the concentration of Cr in YAG-phase is smaller than in Al_2O_3 phase. Finally, new lines, which are coupled to the YAG-phase, appear at low temperature in the highest concentrated ternary eutectics.

Finally, the luminescence, the spectroscopy of the doped Al2O3-YAG and Al2O3-YAG-ZrO2 systems are still in the beginning in comparison with chemical and mechanical properties and research efforts in this field are still very recent. However, from a study of the literature it can be observed that the combination of the oxide eutectic compositions for optics has not yet been explored completely and, we are probably still in the early stage of research in this field.

References

[1] Q. L. Sai, Z. W. Zhao, C. T. Xia, X. D. Xu, F. Wu, J. Q. Ji, L. L. Wang, Ce-doped Al_2O_3-YAG eutectic and its application for white LEDs. Optical Materials., 2013, 35(12), 2155-2159.
[2] S. Q. Song, X. D. Xu, J. Liu, X. S. Bu, D. Z. Li, P. Liu, Y. Z. Wang, J. Xu, K. Lebbou, Structure and white LED properties of Ce-doped YAG-Al2O3 eutectics grown by the micro-pulling-down method, CrystEngComm, 2019, 21, 4545-4550.
[3] H. T. Rocha, L. P. Ferreira, F. J. G, Silva1 Analysis and Improvement of Processes in the Jewelry Industry, Procedia Manufacturing, 2018, 17, 640-644.
[4] F. Bertacchini, E. Bilotta, F. Demarco, P. Pantano, C. Scuro, Multi-objective

optimization and rapid prototyping for jewelry industry: methodologies and case studies, The International Journal of Advanced Manufacturing Technology, 2021, 112(9), 2943-2959.
[5] W. J. Minford, R. C. Bradt, V. S. Stubican. Crystallography and microstructure of directionally solidified oxide eutectics, Journal of the American Ceramic Society, 1979, 62(3-4), 154-154.
[6] O. Benamara, K. Lebbou, Orientations and seed type effect on Al_2O_3-YAG-ZrO_2 eutectic microstructure solidified from the melt by the micro-pulling down technique, Journal of the European Ceramic Society, 2021, 41(11), 5613-5623.
[7] O. Benamara, M. Cherif, T. Duffar, K. Lebbou, Microstructure and crystallography of Al_2O_3–$Y_3Al_5O_{12}$–ZrO_2 ternary eutectic oxide grown by the micropulling down technique, Journal of Crystal Growth, 2015, 429, 27-34.
[8] O. Benamara, K. Lebbou, The impact of the composition and solidification rate on the microstructure and the crystallographic orientations of Al_2O_3–YAG–ZrO_2 eutectic solidified by the micro-pulling down technique, RSC advances, 2021, 11(22), 13602-13614.
[9] V.S. Stubican, R.C. Bradt, Eutectic Solidification in Ceramic Systems, Annual Review of Materials Science., 1981, 11, 267–297.
[10] J.C. Wang, X.Y. Tang, P. Zheng, S.X. Li, T.L. Zhou, R.J. Xie, Self-thermal management YAG:Ce-Al_2O_3 color converters enabling high-brightness laser-driven solid state lighting in a transmissive configuration, Journal of Materials Chemistry C, 2019, 7, 3901-2911.
[11] T. Kang, S. Lee, J. Kim, J. Park, Thermal durability of YAG: Ce ceramic with containing Al_2O_3 and its Raman analysis, Journal of Luminescence, 2020, 222: 117077.
[12] Y. Waku, N. Nakagawa, T. Wakamoto, H. Ohtsubo, K. Shimizu, Y. Kohtoku, High-temperature strength and thermal stability of a unidirectionally solidified Al_2O_3/YAG eutectic composite, Journal of Materials Science, 1998, 33(5), 1217-1225.
[13] L. Carroz, T. Duffar. Tuning the sapphire EFG process to the growth of Al_2O_3/YAG/ZrO_2: Y eutectic, Journal of Crystal Growth, 2018, 489, 5-10.
[14] L. Mazerolles, L. Perriere, S. Lartigue-Korinek, N. Piquet, M. Parlier, Microstructures, crystallography of interfaces, and creep behavior of melt-growth composites, Journal of the European Ceramic Society, 2008, 28(12): 2301-2308.
[15] A. Laidoune, K. Lebbou, D. Bahloul, M. Smadi, M. Zereg, Yttria stabilized Al_2O_3–ZrO_2 eutectic crystal fibers grown by the laser heated pedestal growth (LHPG) method, Optical Materials, 2010, 32(7), 731-734.
[16] M.C. Mesa, S. Serrano-Zabaleta, P.B. Oliete, A. Larrea, Microstructural stability and orientation relationships of directionally solidified Al_2O_3-$Er_3Al_5O_{12}$-ZrO_2 eutectic ceramics up to 1600° C, Journal of the European Ceramic Society, 2014, 34(9), 2071-2080.
[17] O. Benamara, K. Lebbou, Shaped ceramic eutectic plates grown from the melt and their properties, Journal of Crystal Growth, 2016, 449, 67-74.
[18] R. P. Ingel, D. Lewis. III, Lattice parameters and density for Y_2O_3-stabilized ZrO_2, Journal of the American Ceramic Society, 1986, 69(4), 325-332.

[19] J. A. Krogstad, M. Lepple, Y. Gao, D. M. Lipkin, C. G. Levi, Effect of yttria content on the zirconia unit cell parameters, Journal of the American Ceramic Society, 2011, 94(12), 4548-4555.
[20] J. H. Lee, A. Yoshikawa, T. Fukuda, Y. Waku, Growth and characterization of $Al_2O_3/Y_3Al_5O_{12}/ZrO_2$ ternary eutectic fibers, Journal of crystal growth, 2001, 231(1-2), 115-120.
[21] J.H. Lee, A. Yoshikawa, H. Kaiden, K. Lebbou, T. Fukuda, D.H. Yoon, Y. Waku, Microstructure of Y_2O_3 doped Al_2O_3/ZrO_2 eutectic fibers grown by the micro-pulling-down method, Journal of Crystal Growth, 2001, 231(1-2), 179-185.
[22] F.J. Ester, A. Larrea, R.I. Merino, Processing and microstructural study of surface laser remelted Al_2O_3–YSZ–YAG eutectic plates, Journal of the European Ceramic Society, 2011, 31(7), 1257-1268.
[23] X. Wang, Y. J. Zhong, Q. Sun, Y. R. Li, W. Zhang, D. Q. Qi, D, Wang, B. L. Jiang, Crystallography and interfacial structure in a directionally solidified $Al_2O_3/Y_3Al_5O_{12}/ZrO_2$ eutectic crystal, Scripta Materialia, 2018, 145, 23-27.
[24] X. S. Fu, G. Q. Chen, Y. F. Zu, J. T. Luo, W. L. Zhou, Microstructure refinement approaches of melt-grown Al_2O_3/YAG/ZrO_2 eutectic bulk, Ceramics International, 2013, 39(7), 7445-7452.
[25] Vauquelin, Parmentier, Déyeux et Bouillon-Lagrange
Journal de la Société des Pharmaciens de Paris, 1997, 126, 174-176

[26] K. Song, J. Zhang, X. J. Jia, H. J. Su, L. Liu, H. Z. Fu, Longitudinal cross-section microstructure of growth striation in $Al_2O_3/Y_3Al_5O_{12}/ZrO_2$ directionally solidified eutectic ceramic prepared by laser floating zone, Journal of the European Ceramic Society, 2013, 33(6), 1123-1128.
[27] J. LLorca, V. M. Orera, Directionally solidified eutectic ceramic oxides, Progress in materials science, 2006, 51(6), 711-809.
[28] H. J. Su, J. Zhang, C. J. Cui, L. Liu, H. Z. Fu, Rapid solidification of $Al_2O_3/Y_3Al_5O_{12}/ZrO_2$ eutectic in situ composites by laser zone remelting, Journal of Crystal Growth, 2007, 307(2), 448-456.
[29] D. Reinen. Ligand-field spectroscopy and chemical bonding in Cr^3+-containing oxidic solids. Structure and bonding, 1969, 6, 30-51.
[30] R. G. Burns. Mineralogical applications of crystal eld theory, volume 5. Cambridge
University Press, 1993.
[31] J. I. Pena, M. Larsson, R. I. Merino, I. de Francisco, V. M. Orera, J. LLorca, J. Y. Pastor, A. Martin, J. Segurado, Processing, microstructure and mechanical properties of directionally-solidified Al_2O_3–$Y_3Al_5O_{12}$–ZrO_2 ternary eutectics, Journal of the European ceramic society, 2006, 26(15), 3113-3121.
[32] B.M. Epelbaum, A. Yoshikawa, K. Shimamura, T. Fukuda, K. Suzuki, Y. Waku, J. Crystal Growth, 1999, 198/199, 471-475.
[33] J.H. Lee, A. Yoshikawa, S.D. Durbin, D.H. Yoon, T. Fukuda, Y. Waku, J. Crystal

Growth, 2001, 222 791-796.
[34] J.H. Lee, A. Yoshikawa, H. Kaiden, T. Fukuda, D.H. Yoon, Y. Waku, J. Crystal Growth 2001, 231, 179-185.
[35] L. Mazerolles, N. Piquet, M. F. Trichet, L. Perrière, D. Boivin, M. Parlier, New microstructures in ceramic materials from the melt for high temperature applications, Aerospace science and technology, 2008, 12(7),499-505.
[36] J. He, D. R. Clarke, Polarization Dependence of the Cr^{3+} R-Line Fluorescence from Sapphire and Its Application to Crystal Orientation and Piezospectroscopic Measurement, Journal of the American Ceramic Society, 1997, 80(1), 69-78.
[37] A. J. Pardo, R. I. Merino, V. M. Orera, J. I. Pena, Piezospectroscopic study of residual stresses in Al_2O_3–ZrO_2 directionally solidified eutectics, Journal of the American Ceramic Society, 2000, 83(11), 2745-2752.
[38] A. Sayir, S. C. Farmer, The effect of the microstructure on mechanical properties of directionally solidified Al_2O_3/ZrO_2 (Y_2O_3) eutectic, Acta materialia, 2000, 48(18-19), 4691-4697.
[39] O.A. Capeloto, N E de Souza, Santos I A, et al. Preparation, structural and spectroscopic study of sol‐ gel‐ synthesized Cr^{3+}:Al_2O_3 powder. SN Applied Sciences, 2019, 1(12), 1-7.
[40] P R Wamsley and K L Bray. The effect of pressure on the luminescence of Cr^{3+}: YAG. Journal of luminescence, 1994, 59(1-2), 11-17.
[41] R.C. Powell, B.DiBartolo, B. Birang B, et al. Fluorescence studies of energy transfer between single and pair Cr^{3+} systems in Al_2O_3. Physical Review, 1967, 155(2), 296.
[42] S. Geller, Crystal chemistry of the garnets, J. Zeitschrift für Kristallographie-Crystalline Materials, 1967, 125(1-6), 1-47.
[43] T.H. Maiman, R H, Hoskins, I J D'Haenens, et al. Stimulated optical emission in fluorescent solids. II. Spectroscopy and stimulated emission in ruby. Physical Review, 1961, 123(4), 1151.
[44] V. Mykhaylyk, H. Kraus, Y. Zhydachevskyy, et al. Multimodal non-contact luminescence thermometry with Cr-doped oxides. Sensors, 2020, 20(18), 5259.
[45] A.P. Vink and A. Meijerink Electron-phonon coupling of Cr^{3+} in YAG and YGG, J. of Luminescence, 2000, 87-89, 601-604
[46] Y.R. Shen, KL. Bray K.L. Effect of pressure and temperature on the lifetime of Cr3+ in yttrium aluminum garnet Phys. Rev. B 1997, 56, 10882
[47] S. Agachi, Luminescence spectroscopy of Cr^{3+} in Al_2O_3 polymorphs, Optical Materials 2021,114, 111000
[48] R. Wannemacher and J. Heber Cooperative Emission of Photons by Weakly Coupled Chromium Ions in $A1_2O_3$ Z. Phys. B - Condensed Matter 1987, 65, 491-501.